Journal of Hazardous Materials 334 (2017) 212–222

Contents lists available at ScienceDirect

Journal of Hazardous Materials

journal homepage: www.elsevier.com/locate/jhazmat

Enhanced adsorption of bromate from aqueous solutions on ordered mesoporous Mg-Al layered double hydroxides (LDHs)

Huashun Ji [1], Wenhao Wu [1], Feihu Li *, Xiaoxue Yu, Jingjing Fu, Luyao Jia

CICAEET Center, AEMPC Lab, School of Environmental Science and Engineering, Nanjing University of Information Science and Technology, 219 Ningliu Road, Nanjing 210044, China

HIGHLIGHTS

- A facial method for preparation of ordered mesoporous Mg-Al LDH was presented.
- The mesoporous Mg-Al LDH has a high surface area (126 $m^2 g^{-1}$).
- The mesoporous Mg-Al LDH shows a high adsorption capacity for bromate uptake.
- Bromate adsorption mechanism involves both anion-exchange and reconstruction.

GRAPHICAL ABSTRACT

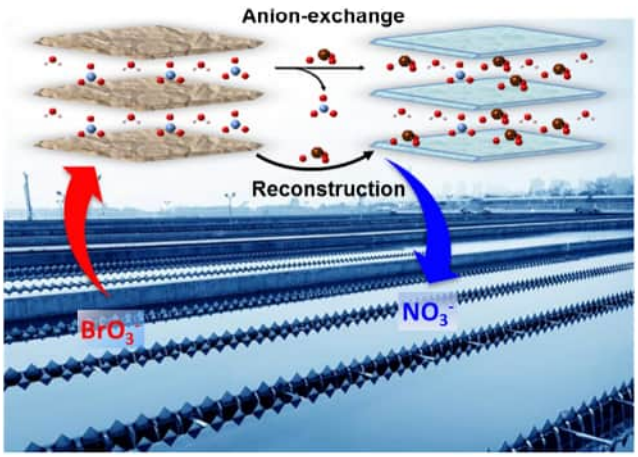

ARTICLE INFO

Article history:
Received 28 December 2016
Received in revised form 3 April 2017
Accepted 5 April 2017
Available online 6 April 2017

Keywords:
Bromate
Layered double hydroxides
Mesoporous
Anion-exchange
Reconstruction

ABSTRACT

An ordered mesoporous Mg-Al layered double hydroxide (meso-LDH350) with a fairly high Brunauer-Emmett-Teller (BET) surface area (126 $m^2 g^{-1}$) has been facilely synthesized and then evaluated for the adsorptive removal of bromate from aqueous solutions. Adsorbents were characterized by a variety of techniques (e.g., XRD, FTIR, SEM, TG-DSC, N_2 physisorption, XPS, etc.). The adsorption studies indicated that the presence of background electrolytes and competitive anions can obviously repress the uptake of bromate on LDHs. The adsorption isotherms agree well with the Langmuir model, giving a maximum adsorption capacity of 59.34 mg g^{-1} (pH 7.5, 10 °C) for meso-LDH350, which is much higher than other LDH-type adsorbents reported in literature. The adsorption kinetic data can be well fitted with the pseudo-second-order rate model. Based on the macroscopic and microscopic studies, bromate adsorption on meso-LDH350 was associated with two mechanisms: the reconstruction of the layered structures of meso-LDH350 and the anion-exchange between bromate and the intercalated anions.

1. Introduction

Bromate (BrO_3^-) is an oxyhalide that was generally formed as one of typical disinfection by-products (DBPs) during the ozonation of bromide-containing water [1]. Bromate has potential carcino-

* Corresponding author.
E-mail address: favorlee@163.com (F. Li).
[1] These authors contributed equally to this work.

http://dx.doi.org/10.1016/j.jhazmat.2017.04.014
0304-3894/

genic properties to induce renal cell tumors, thus increasing the health risks of both humankind and animals [2]. U.S. EPA (1998) and the Ministry of Health of China (2006) had strictly established a maximum contaminant level (MLC) of 10 $\mu g\,L^{-1}$ for bromate in drinking water. Efficient removal of bromate from drinking water is therefore of particular significance with respect to reducing bodies exposure to BrO_3^--contaminated water. Currently, it remains a big challenge to remove bromate efficiently from aqueous solutions because bromate is highly soluble and stable in water. A wide variety of techniques have been developed to sequester bromate from surface waters, including activated carbon adsorption [3], anion-exchange [4–7], biodegradation [8], zero-valent iron reduction [9], catalytic hydrogenation reduction [10] and photocatalytic reduction [11]. Of these technologies, adsorption or anion-exchange with inorganic materials, such as layered double hydroxides (LDHs), has attracted intensive attention due to high effectiveness and low cost [12].

LDHs are composed of stacks of positively-charged, mixed metal hydroxide layers between which are sandwiched of water molecules and various anionic species that are exchangeable with other aqueous anions in the bulk solution, allowing LDHs to be one of the most efficient anion-exchangers for sequestration of toxic anions [13]. As summarized by Goh et al. [12], LDHs have been widely used to adsorb a wide range of anions from water, which consequently allows them to be an alternative adsorbent or anion-exchanger to scavenge bromate in aqueous solution [4–7]. Chitrakar had examined the adsorption of bromate on both Fe(II)-Al LDH (Cl) and Fe(II)-Al LDH (SO_4) and found that bromate would be reduced by structural Fe(II) into bromide, resulting in collapse of the layered structure of LDHs [14,15]. To avoid the structural collapse of LDHs during the removal of bromate, nonferrous LDHs such as Mg-Al LDH [4–7], and Zn-Al LDH [16–18] are preferred to be employed.

It is obvious that the anion-exchange capacity of LDHs is correlated to the anions electrostatically attached on the exchanging sites in the interlayers of LDHs [19]. Besides, surface adsorption on the specific adsorption sites also played a crucial role in anions uptake by LDHs with well-defined pores [20]. How to increase the density of binding sites in LDHs for enhanced uptake of toxic anions is still an open question. Recently, it was reported that layered Mg-Al hydrous oxides (an analog of LDHs) with well-developed mesopores have a high adsorption capacity and affinity towards arsenate species and other toxic anions (e.g., fluoride, bromate, selenate, etc.) [5]. Is it possible to introduce mesopores into LDHs structure for creating more binding sites for toxic anions (e.g., bromate) clean-up? This question is the initial motivation of current work. Mesoporous metal and bimetallic oxides and oxyhydroxides have been, in fact, extensively prepared by using a number of surfactant templates (e.g., cationic, anionic, neutral block copolymers) over the last two decades [21–24]. In the case of preparation of mesoporous and/or mesostructured Mg-Al LDHs, neutral block copolymers (e.g., Pluronic® F-127 or P-123) was more preferable than anionic surfactants since the latter is more likely to intercalate into LDHs as guest anions [25].

In this study, a facile method combining fast co-precipitation and calcination for the synthesis of mesoporous Mg-Al LDH with high adsorption capacity for bromate was presented. The structural properties of mesoporous LDH and its non-mesoporous counterparts were well characterized prior to a series of batch adsorption experiments for bromate uptake. In terms of the results of both batch experiments and molecular spectroscopies, the adsorption mechanisms were also proposed.

2. Experimental section

2.1. Chemicals

All chemicals were of A.R. grade and used without further purification. Magnesium nitrate hexahydrate ($Mg(NO_3)_2{\cdot}6H_2O$, 99%) and aluminum nitrate nonahydrate ($Al(NO_3)_3{\cdot}9H_2O$, 98%) were purchased from Sinopharm Chemical Reagent Co., Ltd. (Shanghai, China). Pluronic F127 was obtained from Sigma-Aldrich Co. (Shanghai, China). Milli-Q ultrapure (18.2 MΩ-cm) water was used to prepare solutions. Bromate stock solution (0.1 M) was prepared by dissolving certain amount of G.R. grade sodium bromate ($NaBrO_3$, Sinopharm Chemical) with ultrapure water and stored in refrigerator (4 °C).

2.2. Preparation of mesoporous LDHs

Mesoporous Mg-Al LDH was prepared by a modified co-precipitation method [26] and followed by calcination. Briefly, 2.4 g of the F127 was dissolved with 120 mL of deionized water under vigorous stirring in a waterbath (60 °C). Then, a mixture of $Mg(NO_3)_2{\cdot}6H_2O$ (12.3 g, 48 mmol) and $Al(NO_3)_3{\cdot}9H_2O$ (9.02 g, 24 mmol) was added into the above solution and stirring until fully dissolved. The mixture was then co-precipitated by dropwise addition of NaOH solution (1 M) until pH ~ 10. To precipitate all aluminum salt, pH was maintained by intermittently adding dilute NaOH (0.2 M) in the following 2 h. After reaction, the resultant white suspensions was treated ultrasonically at 60 °C for 1 h, and then statically aged for 2 h. The as-made white powders were collected by centrifugation and rinsed thoroughly with deionized water for several times, followed by freeze-drying under vacuum overnight. The residual F127 in as-made LDHs was removed by calcination at 350 °C for 3 h in air, giving the mesoporous LDH termed as meso-LDH350. For comparison, two Mg-Al LDH counterparts were also prepared following the same procedure in the absence of F127, and termed as LDH (i.e., the as-made sample) and LDH350 (i.e., the calcinated sample), respectively.

2.3. Characterization of mesoporous LDHs

X-ray diffraction (XRD) analyses of these Mg-Al LDHs were conducted on an XRD-6100 diffractometer (Shimadzu, Japan) at a tube voltage of 40 kV and a tube current of 30 mA with Cu-Kα radiation (λ = 1.5418 Å, step size: 0.02°, scanning rate: 5°/min). Scanning electron micrography (SEM) was recorded by using a Hitachi SU1510 microscope at an accelerating voltage of 1.5 kV. Brunauer-Emmett-Teller (BET) surface area of LDHs was determined by N_2 adsorption at −196 °C using a Quantachrome gas adsorption analyzer (iQ-AG-MP). Prior to BET measurement, the samples were degassed at 80 °C for at least 6 h. Fourier transform infrared (FTIR) spectroscopy was performed on a NIKOLET iS5 spectrometer (Thermo Fisher, USA) following the KBr–pressed–disc method. Thermogravimetry-differential scanning calorimetry (TG-DSC) analysis was carried out on LABSYS EVO TG-DTA/DSC (SETARAM, France) apparatus. Zeta (ζ) potential data were collected on a Zetasizer Nano ZS 90 apparatus (Malvern, UK) using 0.1 mM of $NaNO_3$ solution as background electrolyte. UV–visible diffuse reflection spectra (UV–vis DRS) were obtained from dry-pressed disk samples using a UV–visible spectrophotometer (Cary 100, Agilent, USA) with $BaSO_4$ as the reflectance sample. X-ray photoelectron spectroscope (XPS) (PHI 5000 Versa Probe, UIVAC-PHI, Japan) equipped with a monochromatized Al Kα X-ray source ($h\nu$ = 1486.6 eV) and a hemispherical electron analyzer was used to analyze the surface properties of samples. The C_{1s} peak (284.6 eV) was used for the calibration of binding energy values.

2.4. Batch adsorption experiments

All batch experiments were performed at room temperature (*ca.* 25 °C) unless otherwise stated. Briefly, the adsorption slurries were prepared in 15-mL capped polyethylene centrifuge tubes (Corning, USA) by combining 10 mg adsorbents with a desired volume (e.g., 7.8 μL for pH envelope experiments, giving a final concentration of 1 ppm bromate) of diluted bromate stock solution (0.01 M) and a background electrolyte solution (e.g., 1 mM $NaNO_3$), giving a total volume of 10 mL mixture. After adjusting pH with dilute HNO_3 and NaOH, the slurries (10 mL) were bubbled with pure N_2 for 5 min to exclude dissolved CO_2 and then rotated on a Labquake tube rotator (Thermo Scientific, USA) for 24 h in a thermostatic chamber. The supernates were collected by centrifugation (12000 rpm for 15 min) and filtration with 0.45 μm PES filter (Navigator, Tianjin) for the measurement of bromate concentration by ionic chromatography (IC). Adsorption isotherms were obtained by varying the initial bromate concentration in the range of 1.0 −100 mg L^{-1} (7.82–782 μM) with a constant adsorbent dosage (1 g L^{-1}) and pH (i.e., 7.5 ± 0.2) at 10 °C and 30 °C, respectively. The Langmuir and the Freundlich models as given in Eqs. (1) and (2) were employed to fit the experimental data.

Langmuir model:

$$q_e = \frac{bq_m C_e}{1 + bC_e} \quad (1)$$

Freundlich model:

$$q_e = K_f C_e^{1/n} \quad (2)$$

where q_e (mg g^{-1}) is the adsorption capacity at equilibrium, C_e is the equilibrium BrO_3^- concentration in mg g^{-1}, q_m is the maximum adsorption capacity in mg g^{-1}, b (L mg^{-1}) is Langmuir constant related to adsorption energy; n and K_f are the Freundlich constant.

The competitive effects of co-anions including Cl^-, NO_3^-, SO_4^{2-}, CO_3^{2-}, PO_4^{3-}, were also investigated individually. Stock solutions of these anions were prepared by dissolving a certain amount of their sodium salts (except for Na_2HPO_4) in deionized water. The initial concentration of these anions has been set as same as that of bromate (0.1 mM). The competitive experiments were conducted individually at pH 7.5 ± 0.2 and 25 °C. The pH of the solutions was measured by using a Sartorius pH meter (PB-10) calibrated with standard pH 4.00, 7.00 and 10.01 buffers (Thermo, USA).

2.5. Adsorption kinetic tests

The adsorption kinetics tests were performed at pH 7.5 ± 0.2 and 25 °C with an initial bromate concentration of 10 mg L^{-1} (78.2 μM) and an adsorbent dosage of 1 g L^{-1} in a three-necked flask that loaded with 500 mL of slurries completely mixed by an electrical stirrer (stirring rate: 120 rpm). At varying time intervals 2 mL of solution was collected using a pipette and filtered for analysis of bromate concentration. Both pseudo first-order kinetic model (Eq. (3)) [27] and second-order kinetic model (Eq. (4)) [28] as given below were used to fit the adsorption kinetic data.

$$q_t = q_e(1 - e^{-k_1 t}) \quad (3)$$

$$q_t = \frac{k_2 q_e^2 t}{1 + q_e k_2 t} \quad (4)$$

where q_e (mg g^{-1}) and q_t (mg g^{-1}) are adsorption capacity at equilibrium and contact time t (min), k_1 and k_2 is the pseudo first-order and second-order kinetic rate constants, respectively [29].

2.6. Analysis of bromate

The concentration of BrO_3^- ions were measured by using an ion chromatographer (Dionex, ICS-2000, USA). Samples were filtered with 0.45 μm filter to remove adsorbents and then separated on a Dionex IonPac AS11-HC capillary column (4.0 mm × 250 mm) with 10 mM KOH delivered at a flow rate of 1.0 mL/min. The separation column was operated at 30 °C.

3. Results and discussion

3.1. Characterization of Mg-Al LDHs

Fig. 1A presents XRD patterns of all Mg-Al LDHs, i.e., meso-LDH350, LDH350 and LDH. The reflections of LDH at $2\theta = 11.1°$, 22.2°, 34.6°, 38.6°, 45.8° and 60.4° are corresponding to (003), (006), (009)/(012), (015), (018), and (110) planes respectively, which are typical Miller-Bravais indices of poorly crystallized Mg-Al LDH (NO_3) phase [30]. The *d* spacing of (003) reflection is 7.8 Å, indicating that nitrate (NO_3^-) is the predominant guest anions intercalated in the interlayers of Mg-Al LDHs [31]. Upon calcination at 350 °C, the intensity of all reflections were decreased due to the loss of interlayer water molecules and the partial dehydroxylation of the double hydroxide sheets as verified by the reflections of MgO (JSPDS PDF# 01-1235) in both patterns of meso-LDH350 and LDH350 [32]. It is worth to note that the introduction of F127 into the synthetic recipe seems not to affect the lamellar structure of LDHs since the relative positions of all reflections showed no obvious shifts, which implies that the characteristic layered structure of LDHs was preserved after calcination. It is evident that the LDH particles aggregated to form larger particles during the calculation treatment, and that this aggregation process was more obvious in the presence of F127 (Table S1 in the Supplementary data).

The FTIR spectra of Mg-Al LDHs are given in Fig. 1B. The broad band at 3450 cm^{-1} is attributed to the stretching of O—H groups associated with the interlayer water molecular or O—H groups in adjacent layers. The band at 1637 cm^{-1} is assigned to the deformation vibration of H—O—H (δ_{H2O}) of interlayer water molecules [33]. As expected, the intensities of the above two band were slightly decreased after calcination due to the loss of interlayer water. The band at 1384 cm^{-1} refers to the antisymmetric stretching vibration (ν_3 mode) of both nitrate (ν_{NO3}) and carbonate (ν_{CO3}) [6,32,34]. The bands observed in the range of 500−800 cm^{-1} are generally assignable to M—O, O—M—O and M—O—M (M = Mg, Al) lattice vibrations [35,36]. Additional, a weak shoulder band assignable to the stretching vibration (ν_2 mode) of CO_3^{2-}(ν_{CO3}) was also observed at 833 cm^{-1}, which was probably caused by the exposure of LDHs to the atmosphere during storage [33,34]. Furthermore, neither stretching vibration bands of C—O groups (*ca.* 1060 cm^{-1}) nor vibration bands of —CH_2CH_2 groups (*ca.* 2820 and 2910 cm^{-1}) was observed, indicating that calcination at 350 °C can efficiently remove F127 from the as-made mesoporous LDH.

Fig. 1C depicts the TG-DSC curves of as-made mesoporous LDH. It is clear to note that the thermogravimetric (TG) curve shows three mass loss steps: the first refers to the range below ~230 °C, the second and the third steps were located in ~ 230–421 °C and ~421–519 °C, respectively. The first mass loss interval (18.6 wt.%) was assigned principally to hydration water and physisorbed water [37]. The second mass loss interval where 18.5 wt.% was lost, corresponded to the partial dehydroxylation of the layers, the pyrolysis of the intercalated nitrate and F127 [38]. In the last step, mass loss (6.6 wt.%) was probably contributed from partial dehydroxylation and pyrolysis of the residual F127 and nitrate. Calcination of the as-made mesoporous LDH at a desired temperature is crucial for the integrity of layered structure of LDHs [4,30,33,38]. Our

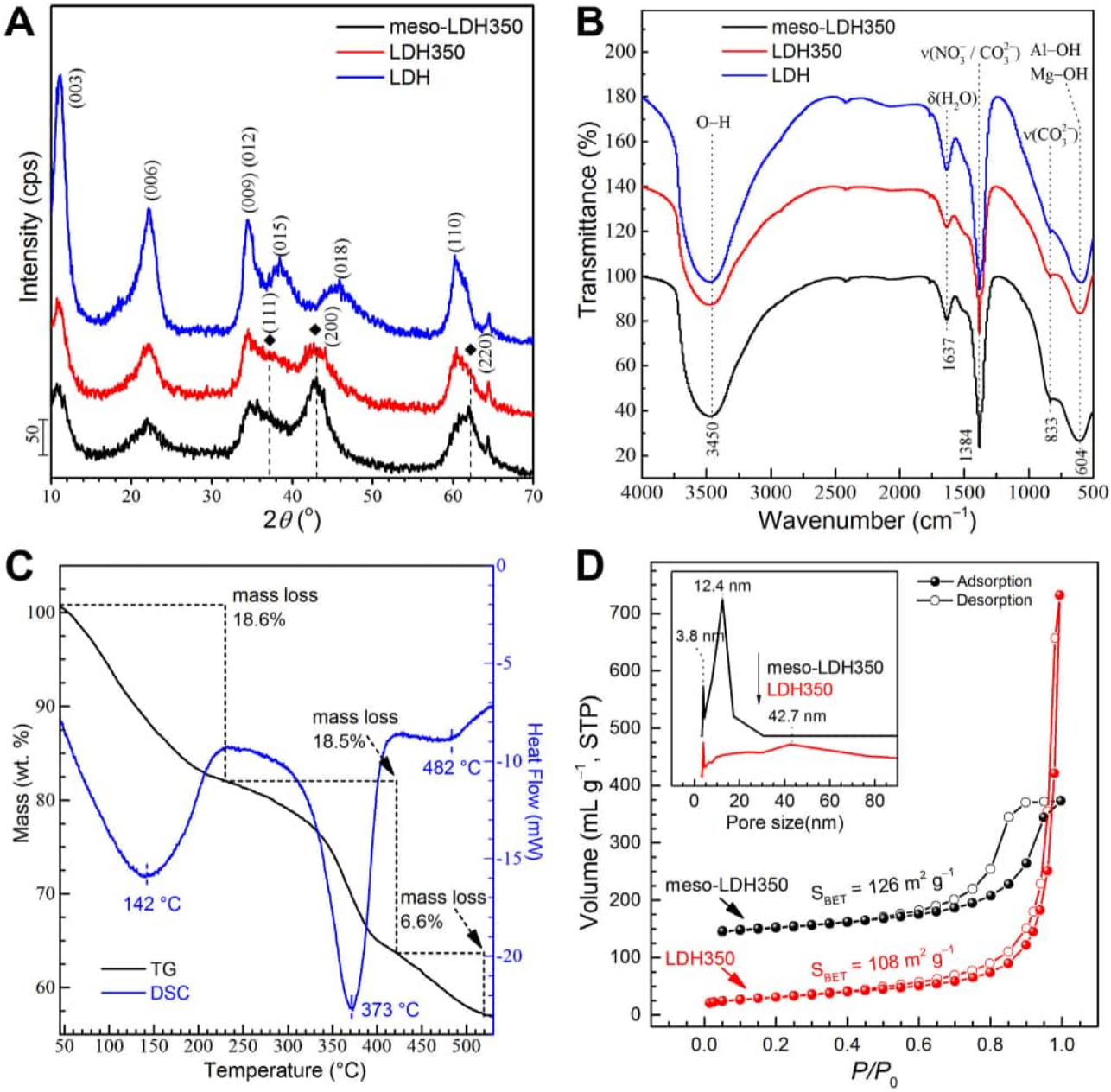

Fig. 1. Characterizations of synthetic Mg-Al LDHs: (A) XRD patterns. Noted that MgO (JCPDS # 01-1235) phase was marked with diamonds (♦); (B) FTIR spectra; (C) TG-DSC curves of as-made meso-LDH; (D) N_2 adsorption-desorption isotherms of meso-LDH350 and LDH350 at −196 °C. Inset is the corresponding BJH pore size distribution graphs.

attempts to calcinate the as-made mesoporous LDH above 350 °C has led to a structure-collapsed sample without any mesopores (data not shown), consistent with previous report that the structural collapse took place at around 360 °C for Mg-Al LDHs [30]. It should be stressed that, in our case, calcination at 350 °C would not only allow the lamellar structure of LDHs to survive, but also efficiently promote the formation of mesoporous structure and MgO that crystallizes approximately at 400 °C in F127-free Mg-Al LDHs [30].

The nitrogen adsorption-desorption isotherms and corresponding pore size distribution of meso-LDH350 and LDH350 are shown in Fig. 1D. The pore size distributions (PSD) of both samples were calculated with the Barrett-Joyner-Halenda (BJH) method using the desorption data of the isotherms. The adsorption-desorption isotherm of meso-LDH350 can be classified as type IV (IUPAC classification) with a hysteresis loop of type H2 at high relative pressures (P/P_0 = 0.6–1.0), which implies that the mesoporous structure was ink-bottle-type mesopores [39]. Correspondingly, meso-LDH350 shows a bimodal pore size distribution (upper curve, inset of Fig. 1D), a uniform pore at the mean value of 12.4 nm along with another narrow uniform pore at the mean value of 3.8 nm. The isotherm of LDH350 exhibits a type II isotherm with a hysteresis loop of type H3 according the IUPAC classification. This type of loop are derived from the macropores that are formed by non-rigid aggregates of plate-like particles [40], which agrees well with the corresponding pore size result (lower curve, inset of Fig. 1D) showing a broad PSD curve spanning over the macroporous range. The Brunauer-Emmett-Teller (BET) surface area of meso-LDH350 and LDH350 are about 126 $m^2\ g^{-1}$ and 108 $m^2\ g^{-1}$, respectively, much greater than that of Mg-Al LDH synthesized via the hydrothermal method [41].

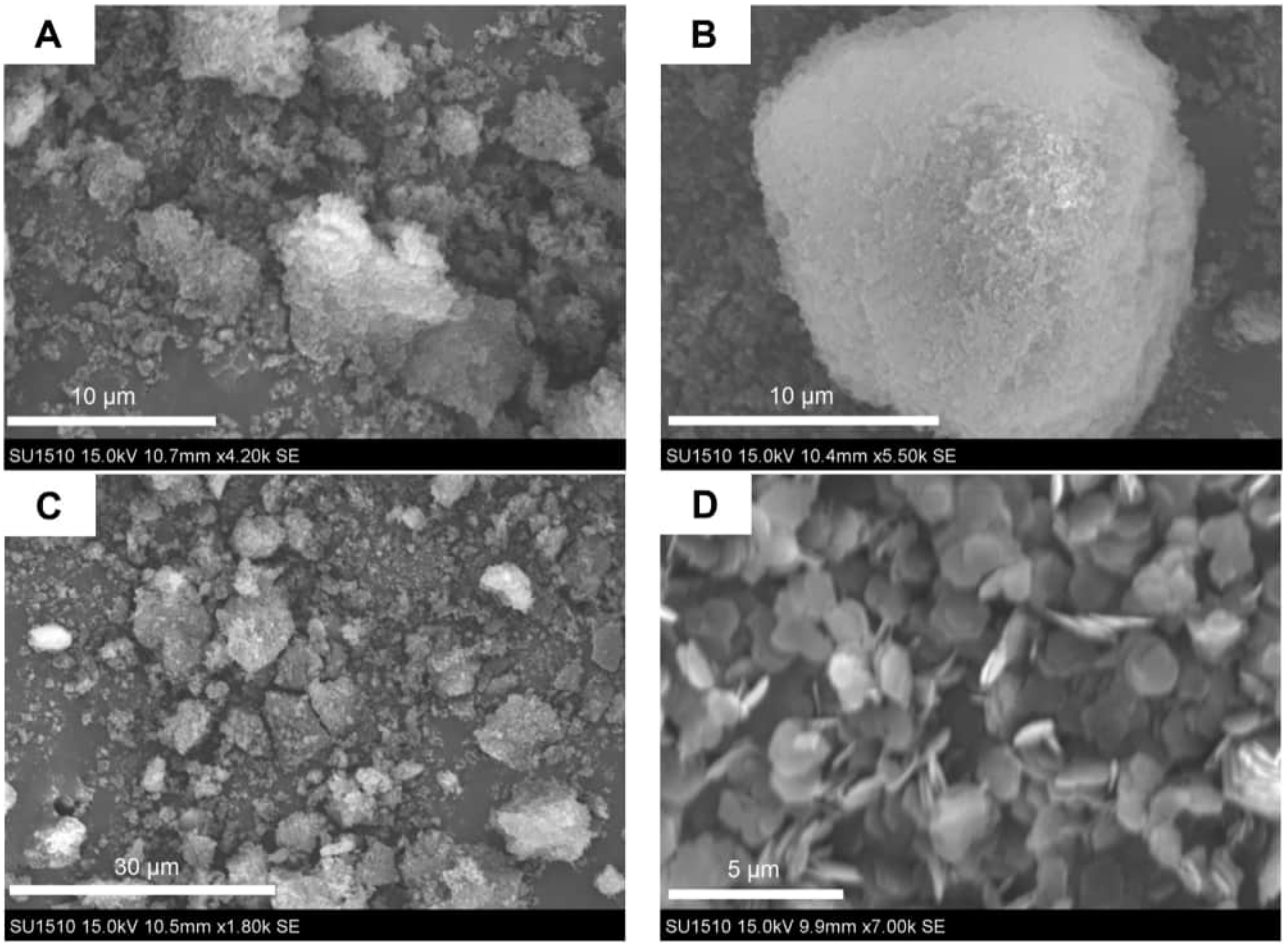

Fig. 2. SEM images of synthetic Mg-Al LDHs: (A) meso-LDH350, (B) LDH350, (C) LDH and (D) LDH synthesized via the hydrothermal method [41].

The morphologies of LDH samples were characterized by SEM images presented in Fig. 2. The morphological features of the LDH samples are quite similar irrespective of the addition of F127, consisting of particulate aggregates with irregular shapes and sizes ranged from several to tens of micrometers (Fig. 2A–C), which are totally different from the flake-like particles of hydrothermal-synthesized Mg-Al LDH (Fig. 2D) [41]. Furthermore, it can be noted that the external surfaces of calcinated LDHs (Fig. 2A, B) are more coarser than that of as-made LDH (Fig. 2C), and that meso-LDH350 are composited of foam-like particles, whereas LDH350 is consisted of agglomerates likely formed as an aggregation of plate-like grains. This observation is in good accordance with the results of N_2 adsorption-desorption isotherms as described above.

3.2. Effect of initial pH and ionic strength

The removal percentages (removal%) of bromate on Mg-Al LDHs at varied ionic strengths as a function of initial pH are given in Fig. 3. As initial pH increased from 2 to 11, the removal percentages of bromate on all LDHs exhibit a similar trend that they increased gradually in acidic pH range until achieved maxima in pH 6–9, and then declined slowly at pH > 9. The pH_{PZC} (point of zero charge) were about 9.5, 10.2, and 11.0 for LDH, LDH350, and meso-LDH350, respectively (Fig. S1 in the Supplementary data). It is expected that LDHs have positive surface charges when pH is below pH_{PZC}, which is favorable for the binding of the negatively charged bromate, and that the surfaces of LDHs become negatively charged when pH is above pH_{PZC} depressing the adsorption of bromate due to the electrostatic repulsion. However, it is shown that the removal% of bromate increased with increasing pH in the pH range of 2–6 ($<pH_{PZC}$) for all LDHs, which is somewhat in contrary to the above expectation. This is possible due to the changes in the solution pH

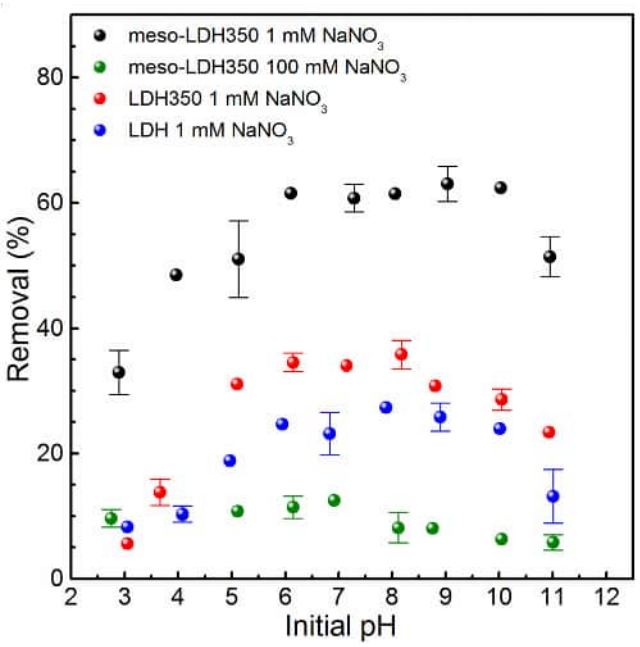

Fig. 3. Effects of initial pH and ionic strength on bromate adsorption on Mg-Al LDHs.

(as shown in Fig. S2), which can increase by 3–5 units from the initial to the equilibrium values during the adsorption processes [17], resulting in a decreased removal% when the equilibrium pH was close to and eventually above pH_{PZC}. Another reason would be the fact that the pHs of all fresh slurries were above 9.0, and more HNO_3 was needed to draw back them to more acidic pHs, which consequently depressed bromate uptake due to the competition from the introduced nitrate [6]. When pH was above pH_{PZC}, the concentration of OH^- increases as pH increases, which results in a decrease in bromate adsorption due to the competitive effect of hydroxides [42]. Moreover, Mg-Al LDH could be partly dissolved at pH > 10 [17], which can also lead to a decrease in removal%. It should be noted that all the equilibrium pHs were above their initial counterparts at pH < 10 (Fig. S2), and the smaller the initial pH was, the more increment was needed to achieve its equilibrium counterpart. This is probably arisen from the consumption of protons and release of hydroxide ions to the solution during the adsorption process as confirmed in the mechanism section. At the ionic strength of 1 mM $NaNO_3$, the removal% of bromate on all LDHs decreased in the order meso-LDH350 » LDH350 > LDH.

Generally, ionic strength dependence (usually 1:1 ionic salts were used as background electrolytes, e.g., $NaNO_3$) of adsorption has been used to indirectly distinguish between inner- and outer-sphere adsorption mechanisms for ions at the solid/aqueous interface [43]. Ions showing little ionic strength dependence of adsorption were considered to form strong inner-sphere surface complexes, whereas ions showing significant ionic strength dependence were regarded as weak attaching as outer-sphere surface complexes. Ions that form weak outer-sphere surface complexes must display decreasing adsorption with increasing ionic strength due to competition from the background electrolyte [43]. Previous study suggested that bromate might predominantly form outer-sphere complexes on LDH [7]. The removal% of bromate on meso-LDH350 dropped down dramatically as the ionic strength increased from 1 mM to 100 mM (Fig. 3), verifying that the mechanism associated bromate adsorption on meso-LDH350 is involved in outer-sphere complexes (anion-exchange) rather than inner-sphere complexes [7].

3.3. Effect of competitive anions

Common anions such as Cl^-, NO_3^-, SO_4^{2-}, CO_3^{2-}, and PO_4^{3-} in surface water might compete with bromate for the binding sites of LDHs [6]. Competitive experiments were performed triply with a [anions]/[bromate] molar ratio of 1.0 and the results are given in Fig. 4. Obviously, the competitive effects of these anions can be ranked in the order sulfate > phosphate > nitrate > carbonate > chloride, which is slightly different with that for nanocrystalline Mg-Al LDH [6]. This might arise from the difference in the pore structure of nanocrystalline Mg-Al LDH and that of meso-LDH350. Nevertheless, due to a higher ionic potential μ (4.90–8.70 nm^{-1}) of bi- and tri-valent anions, bi- and tri-valent anions (e.g., SO_4^{2-}, PO_4^{3-}) are more competitive than monovalent anions (e.g., Cl^-, NO_3^-) with the exception of carbonate. The reason of carbonate showing less influence on bromate adsorption than chloride was probably attributed to the fact that a portion of carbonate from the reaction of atmospheric CO_2 and water has been pre-adsorbed on meso-LDH350 during storage. This is also evidenced by the above FTIR results (Fig. 1B).

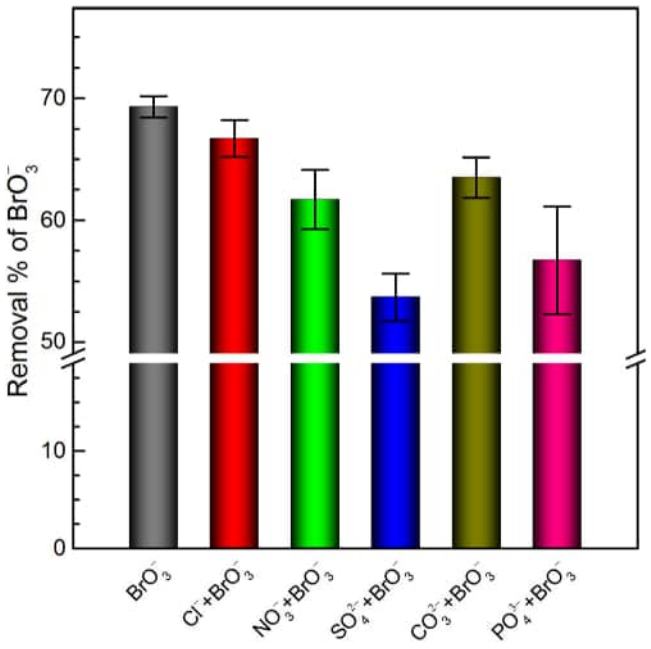

Fig. 4. Effect of competitive anions ([anions]/[bromate] = 1.0) on bromate adsorption on meso-LDH350.

For monovalent anions, chloride was expected to suppress bromate adsorption more heavily than nitrate since lower hydration energy is more favorable for anion-exchange ($\Delta G^\circ_{Cl} < \Delta G^0_{NO3}$) [44]. In contrary, the experimental data suggest that chloride has less influence than nitrate in bromate adsorption, indicating that anion-exchange may not be the only mechanism for bromate adsorption on meso-LDH350. Furthermore, the presence of individual Cl^-, NO_3^-, and CO_3^{2-} (0.1 mM) decreased the removal% of bromate only by 3.8%, 10.9%, and 8.4% respectively (Fig. 4), all far less than 50%, suggesting that bromate has a high affinity to meso-LDH350 and that anion-exchange should not be the only mechanism for bromate adsorption on meso-LDH350.

3.4. Adsorption isotherms

The adsorption isotherms are given in Fig. 5, which were fitted by both Langmuir (solid line) and Freundlich (dotted line) models using nonlinear algorithms (Eqs. (1) and (2)). The fitting parameters are tabulated in Table 1. The greater correlation coefficients (R^2) of the Langmuir model as compared to those of the Freundlich model indicate that the adsorption data are better fitted by the Langmuir model than by the Freundlich model. The maximum adsorption capacities (q_m) at 10 °C calculated by the Langmuir

Table 1
Adsorption isotherm parameters from the Langmuir and Freundlich models' fitting.

Samples	Temperature (°C)	Langmuir			Freundlich		
		q_m (mg g^{-1})	b (L mg^{-1})	R^2	K_F	n	R^2
LDH	10	12.61	0.0606	0.976	1.74	2.42	0.865
	30	14.58	0.0645	0.978	2.12	2.45	0.879
LDH350	10	16.36	0.0696	0.995	2.44	2.44	0.921
	30	25.69	0.0497	0.983	2.85	2.18	0.902
meso-LDH350	10	59.34	0.0383	0.996	4.43	1.81	0.972
	30	54.98	0.0380	0.995	4.21	1.85	0.956

equation (Eq. (1)) were 12.61 mg g^{-1}, 16.36 mg g^{-1}, 59.34 mg g^{-1} for LDH, LDH350 and meso-LDH350 respectively (Table 1). LDH350 exhibited a higher adsorption capability as compared with that of LDH, suggesting that calcination can improve the maximum adsorption capacity. It was found that calcinated LDHs, when contacting with aqueous solutions, usually reconstructed firstly by rehydration of the disordered hydroxide sheets, in which bromate may enter into the interlayers of LDHs [45]. Not surprising, meso-LDH350 exhibited the highest q_m amonge all LDHs in this study, which was contributed to its highest surface area and the mesoporous structure as described above. The high surface area offered abundant binding sites for bromate and the mesoporous networks afforded a plenty of accessible diffusion pathways for bromate. The maximum adsorption capacities of bromate on these LDHs follow the order meso-LDH350 » LDH350 > LDH (Table 1). It should be noted that the q_m of meso-LDH350 decreased with increasing temperature from 10 to 30 °C, whereas the adsorption capacities of both LDH350 and LDH increased with temperature. This is possibly arising from the differences in the pore structures of these LDHs.

For comparison, the maximum adsorption capacities of bromate on other LDH-type adsorbents are summarized in Table 2. Among these adsorbents, meso-LDH350 and LDH350 have maximum adsorption capacities (i.e., 59.34 mg g^{-1} at 10 °C and 25.69 mg g^{-1} at 30 °C respectively) higher than those of other LDHs including hydrothermally-treated Zn-Al LDH (calcinated) [4,18], hydrothermally-treated Zn-Fe(II)-Al LDH [46], hydrothermally-treated Zn-Al LDH (calcinated) [17], hydrothermally-treated Mg-Al LDH [6,7], even some of these LDHs had a higher surface area than both meso-LDH350 and LDH350. When considering the adsorption density ($\Gamma = q_m/S_{BET}$, Table 2), the maximum specific adsorption density of bromate on meso-LDH350 (0.47 mg m^{-2}) is also comparable to that of thermally-treated Mg-Al xerogel (0.5 mg m^{-2}), in which the higher surface area and the hierarchical porous structure (i.e., from macropores to micropores) are believed to contribute to its highest maximum adsorption capacity (78.0 mg g^{-1}) [5]. To evaluate the recycle performance of mesoporous LDH, spent meso-LFH350 (0.22 g) was regenerated by collecting centrifugally and desorbing with a solution (10 mM $NaNO_3$ + 100 mM NaOH, 220 mL), followed by rinsing with ultrapure water several times before next adsorption cycle. The adsorption–regeneration experiments were conducted for five cycles. The removal% of bromate decrease obviously from over 95% to ~40% after five cycles of adsorption-desorption (Fig. S3 in the Supplementary data). This is probably due to the decrease in crystallinity and the collapse of mesoporous structure of meso-LDH350. The recycle performance of meso-LDH350 is not as good as other calcinated LDHs that a thermal regeneration were employed [17,18], implying that the reconstruction of layered structure should contribute in part to the adsorptive removal of bromate by meso-LDH350. Nevertheless, from a practical point of view, meso-LDH350 with such high adsorption capacity is expected to use as an alternative to commercial adsorbents for bromate removal from aqueous solutions.

3.5. Adsorption kinetics

The kinetic curves of bromate adsorption were given in Fig. 6. It was observed that the bromate adsorption capacity (q_t) at time t increased first with the contact time (t) and then attained equilibrium within a certain period of time (<3 h). The calcinated adsorbents, meso-LDH350 and LDH350, exhibited a similar initial rapid uptake of bromate within the first 80 min and 120 min respectively, followed by a slow adsorption process to reach saturation in 2.0–21 h. This type of fast adsorption involving LDHs is believed to be the anion-exchange reactions [4,47]. However, the as-made LDH showed a different kinetics that q_t increased rapidly with contact

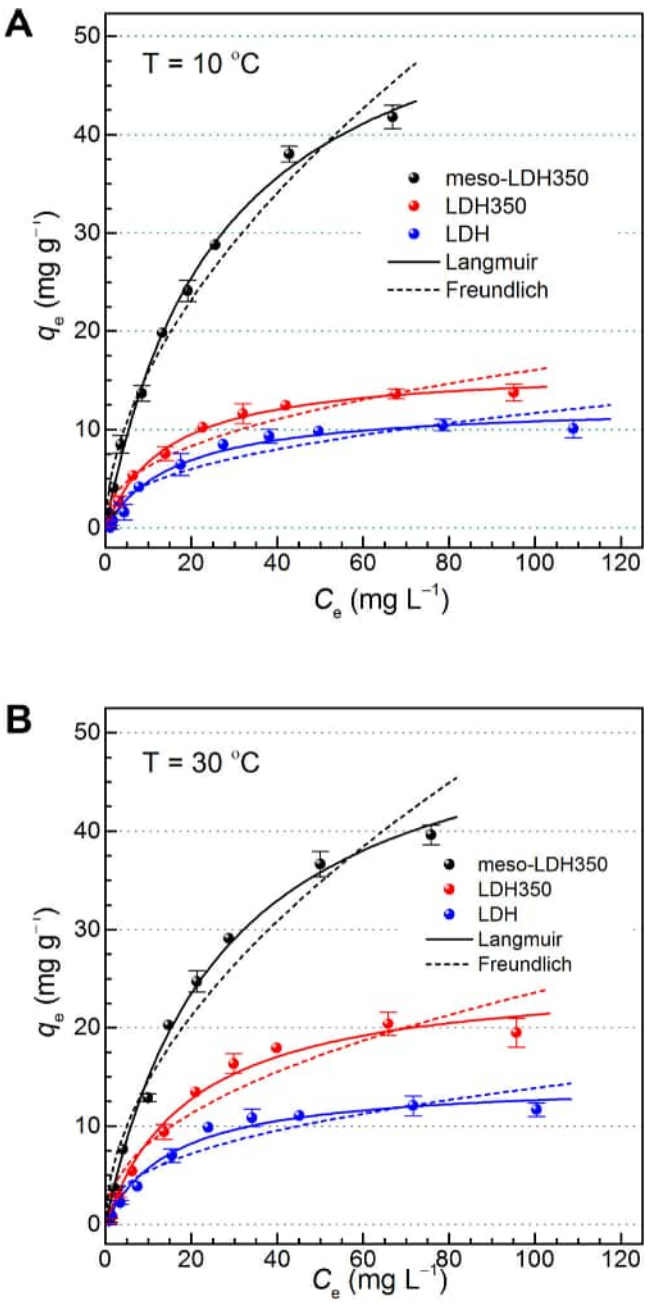

Fig. 5. Adsorption isotherms of bromate on Mg-Al LDHs at (A) 10 °C, and (B) 30 °C.

time until reaching the maximum at $t \sim 20$ min, and then dropped down gradually and attained saturation in 3.0 −10 h (Fig. 6). The discrepancy in kinetics between LDH and the calcined LDHs is probably due to the difference in the pore structures of these adsorbents as desicribed above. There is no need for LDH to reconstruct in the beginning of adsorption, resulting a faster initial adsorption rate as compared to that of calcinated LDHs. As adsorption proceeds, an excess amount of BrO_3^- was likely to attach onto the surface of LDH and further diffused into the interlayers to exchange NO_3^- until a saturation was achieved. The slight decline of q_t in 50–200 min seems to be due to the transition from an initial multilayer attachment to a final favorable monolayer adsorption of BrO_3^-.

No significant changes in q_t were observed from 3.0 to 21 h for all adsorbents, implying adsorption equilibrium was reaching at that time. Chitrakar et al. has also shown longer equilibration time from 48 h to 72 h for bromate adsorption on calcinated Mg-Al LDHs

Table 2
Comparison of the maximum adsorption capacity (q_m) of bromate on *meso*-LDH350 with other LDH-type adsorbents.

adsorbents	BET surface area ($m^2\ g^{-1}$)	initial pH	T (°C)	q_m ($mg\ g^{-1}$)	Γ ($mg\ m^{-2}$)	ionic strength (mM)	ref
hydrothermally-treated Zn-Al LDH (calcinated)	91	6.9	20	0.12	0.001	0	[18]
hydrothermally-treated Zn-Fe(II)-Al LDH	55	7.0	22	0.20	0.004	0	[46]
hydrothermally-treated Mg-Al LDH (calcinated)	200	9.6–9.8	RT[a]	0.99	0.005	0	[4]
hydrothermally-treated Zn-Al LDH (calcinated)	91	6.9	20	1.16	0.01	0	[17]
hydrothermally-treated Mg-Al LDH (FCHT-LDH)	127	9.5	25	12.80	0.10	10.0	[7]
hydrothermally-treated Mg-Al LDH	127	9.5	25	22.40	0.18	0	[6]
thermally-treated Mg-Al LDH xerogel	155	4.5	22	78.0	0.50	10.0	[5]
LDH350	108	7.5	30	25.69	0.24	1.0	This study
meso-LDH350	126	7.5	10	59.34	0.47	1.0	This study

[a] RT refers to room temperature.

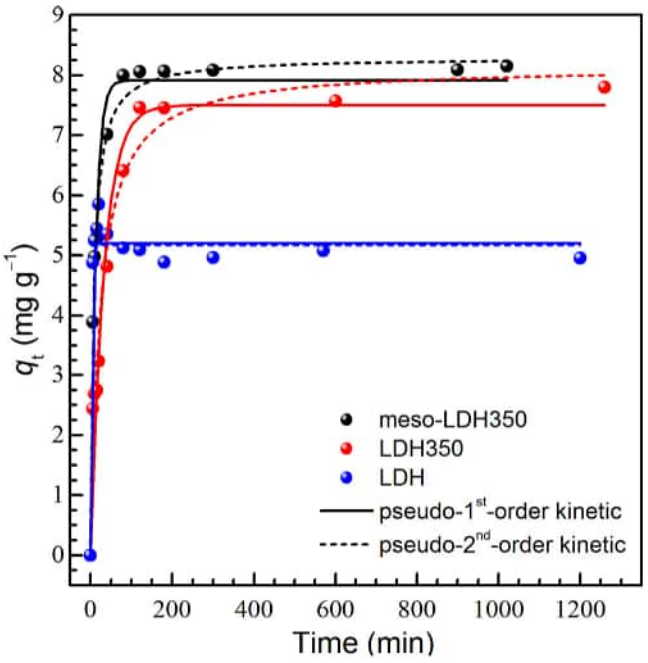

Fig. 6. Adsorption kinetics of bromate on Mg-Al LDHs.

[4]. This indicates that bromate shows faster kinetics onto meso-LDH350 and LDH350, which are also faster than other LDH-type adsorbents, such as calcinated Mg-Al LDH [4], and FCHT-LDH [7]. Considering that the reconstruction of calcined LDHs still takes some time, a 24 h period was therefore believed to be enough to establish equilibrium for bromate adsorption isotherm experiments in our cases.

The experimental data were fitted by both the pseudo-first and the pseudo-second-order rate equations (Eqs. (3) and (4)). The fitting results were summarized in Table 3 and plotted in Fig. 6. The values of q_e calculated from Eq. (4) are 5.17 $mg\ g^{-1}$, 8.14 $mg\ g^{-1}$, and 8.29 $mg\ g^{-1}$ for LDH, LDH350 and meso-LDH350, respectively (Table 3), close to the experimental data (Fig. 6). Comparison of the correlation coefficients (R^2) of both kinetic models indicates that the pseudo-second-order rate model with R^2 above 0.96 is better to fit the kinetica data of all adsorbents, suggesting a chemisorption process occurred.

3.6. Adsorption mechanisms

To elucidate the adsorption mechanism responsible for bromate uptake on meso-LDH350, both fresh and spent adsorbents were collected and handled properly, followed by characterizations with XRD, FTIR, UV–vis DRS and XPS, and the results are given in Fig. 7. It was observed that the intensities of all LDH reflections increased and the reflections of MgO disappeared after adsorption of bromate (Fig. 7A), suggesting that a reconstruction of the layered structure in meso-LDH350 occurred during adsorption. As a consequence, the *d* spacing of (003) reflection recovered from 8.1 Å to 7.8 Å, which is in good agreement to that of FCHT-LDH after adsorption of bromate (i.e., 7.84 Å) [7], implying that bromate was likely to be bond via anion-exchange with the intercalated anions (the remaining NO_3^- and OH^- as evidenced by the FTIR spectra). Nevertheless, a reconstruction mechanism has been identified by Ulibarri and coworkers for the enhanced uptake of anionic pollutants on calcinated LDHs [48]. It is therefore reasonable to suggest that a second mechanism—the reconstruction mechanism should be responsible for the enhanced adsorption of bromate on meso-LDH350. After adsorption, the FTIR band of nitrate at 1384 cm^{-1} weakened a lot and the weak carbonate band at 833 cm^{-1} disappeared, whereas a new band at 791 cm^{-1} contributed to Br—O stretching vibration appeared (Fig. 7B), confirming that anion-exchange has played an important role in bromate adsorption on meso-LDH350. This was also verified by the UV–vis DRS spectra (Fig. 7C), in which two new peaks at 252 nm and 375 nm associated with the electron transition (ET) of bromate (see Fig. S4 in the *Supplementary data*) appeared and the intensity of both 215 nm (assignable to the ET of Mg-Al LDH) [49] and 300 nm (assignable to the ET of NO_3^- to Mg/Al) [50] decreased slightly (inset of Fig. 7C) after adsorption, indicating anion-exchange took place. Fig. 7D presents the survey XPS spectra of meso-LDH350 before and after bromate adsorption. It is noted that, besides the main elements including O, Al, and Mg observed in both spectra, the Br peaks (Br3s, Br3p, and Br3d) appeared in the bromate-adsorbed meso-LDH350 (see also Fig. S5 in the *Supplementary data*), confirming that bromate has been sequestered by meso-LDH350. On the basis of above results, the mechanism of bromate adsorption on meso-LDH350 is contributed both from the reconstruction of the layered structure in meso-LDH350 and from the anion-exchange between bromate in bulk solution and the intercalated anions as given in Eqs. (5)–(9) and illustrated in Fig. 8. When adding fresh meso-LDH350 into bromate-containing solution, the reconstruction occurred likely in a manner that a part of bromate (Eq. (5)), apart from hydroxyls and nitrates (Eqs. (6) and (7)), participated to reconstruct the layered structure, which consequently increases the solution pHs (see also Fig. S2) by consumption of protons and release of hydroxide ions (Eqs. (5)–(7)). It is obvious that the more acidic the solution was, the more rapid the reconstruction reaction was. Meanwhile, a portion of bromate replaced the interlayer anions via anion-exchange (Eqs. (8) and (9)), forming a BrO_3^--intercalated meso-LDH350. Both the higher BET surface area and the mesoporous structure of meso-LDH350 facilitate the efficient and fast removal of bromate in such manners.

Reconstruction:

$$\equiv M{-}O^- + 2H^+ + BrO_3^- \rightarrow \equiv M{-}OH_2^+/BrO_3^- \quad (5)$$

$$\equiv M{-}O^- + 2H_2O \rightarrow \equiv M{-}OH_2^+/OH^- + OH^- \quad (6)$$

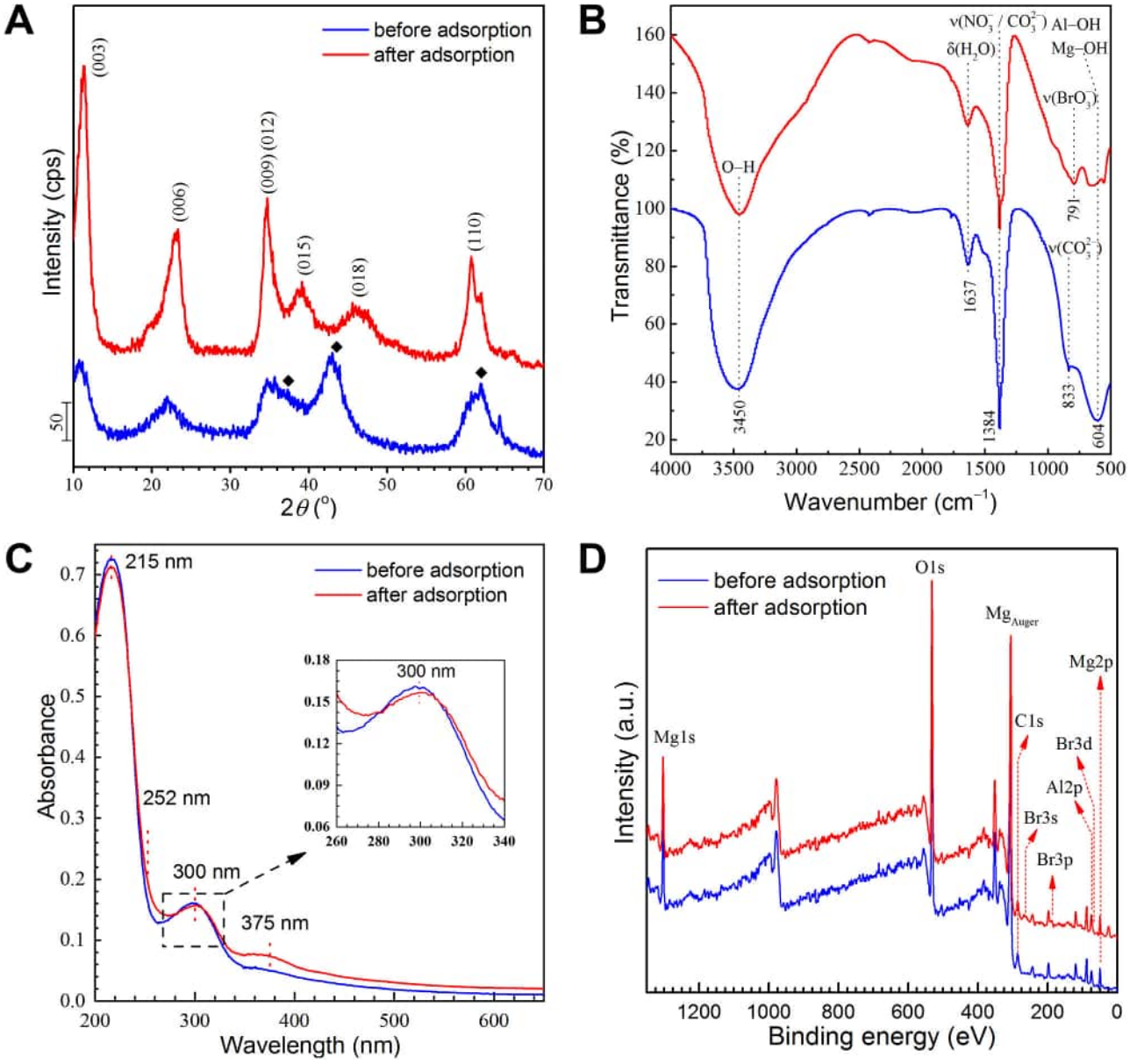

Fig. 7. (A) XRD patterns, (B) FTIR spectra, (C) UV–vis DRS spectra, and (D) XPS spectra of meso-LDH350 before and after adsorption of bromate.

Fig. 8. Schematic illustration of adsorption mechanism for bromate uptake on meso-LDH350.

Table 3
Kinetics parameters from the Pseudo-first-order and Pseudo-second-order rate models' fitting.

Samples	Pseudo-first-order			Pseudo-second-order		
	k_1 (min^{-1})	q_e ($mg\,g^{-1}$)	R^2	k_2 ($g\,mg^{-1}\,min^{-1}$)	q_e ($mg\,g^{-1}$)	R^2
LDH	5.20	0.97	0.927	–	5.17	0.963
LDH350	0.031	7.50	0.955	0.005	8.14	0.966
meso-LDH350	0.083	7.91	0.943	0.017	8.29	0.981

$$\equiv M{-}O^- + 2H^+ + NO_3^- \rightarrow \equiv M{-}OH_2^+/NO_3^- \quad (7)$$

Anion-exchange:

$$\equiv M{-}OH_2^+/NO_3^- + BrO_3^- \leftrightarrow \equiv M{-}OH_2^+/BrO_3^- + NO_3^- \quad (8)$$

$$\equiv M{-}OH_2^+{}_/OH^- + BrO_3^- \leftrightarrow \equiv M{-}OH_2^+/BrO_3^- + OH^- \quad (9)$$

4. Conclusions

In summary, we have presented a facile method for the preparation of mesoporous Mg-Al LDH (termed as meso-LDH350) by fast co-precipitation of Mg-, Al-nitrate precursors and F127 in alkaline solution, followed by calcination. The mesoporous Mg-Al LDH exhibits a pretty high surface area (S_{BET} = 126 $m^2\,g^{-1}$) and foam-like mesopores, which allows it to have a much higher adsorption capacity (59.34 $mg\,g^{-1}$, 10 °C, pH 7.5) and excellent potentiality to sequester bromate from aqueous solution as compared with other LDH-type adsorbents. The adsorption isotherms of meso-LDH350, and its non-mesoporous counterparts, LDH350 and LDH, agree well with the Langmuir algorithm. The kinetic data of bromate adsorption on all adsorbents can be well fitted with the pseudo-second-order rate model. The mechanism for bromate adsorption on meso-LDH350, in terms of the results of XRD, FTIR, UV–vis DRS and XPS, is mainly contributed both from the reconstruction of layered structures in meso-LDH350 and from the anion-exchange between bromate in bulk solution and the intercalated anions. In summary, this work provides a facile approach to prepare ordered mesoporous Mg-Al LDH with a high surface area and a high adsorption capacity for bromate, making it a potential candidate for adsorptive removal of bromate from aqueous solutions.

Acknowledgements

The work was partially supported by National Natural Science Foundation of China (NSFC) (51002080), Nature Science Foundation of Jiangsu (BK20171480), the open fund of AEMPC Lab (KFK1505), SPITP Program (201510300058, 201610300050, 201610300273), Top-notch Academic Programs Project of Jiangsu Higher Education Institutions (PPZY2015C222) and the Priority Academic Program Development of Jiangsu Higher Education Institutions (PAPD). Special thanks are due to Dr. Wonyong Choi and all anonymous reviewers for their helpful comments and suggestions on the earlier version of this paper.

Appendix A. Supplementary data

Supplementary data associated with this article can be found, in the online version, at http://dx.doi.org/10.1016/j.jhazmat.2017.04.014.

References

[1] U. von Gunten, J. Holgne, Bromate formation during ozonation of bromide-Containing waters—interaction of ozone and hydroxyl radical reactions, Environ. Sci. Technol. 28 (1994) 1234–1242.
[2] Y. Kurokawa, A. Maekawa, M. Takahashi, Y. Hayashi, Toxicity and carcinogenicity of potassium bromate—a new renal carcinogen, Environ. Health Perspect. 87 (1990) 309–335.
[3] M.L. Bao, O. Griffini, D. Santianni, K. Barbieri, D. Burrini, F. Pantani, Removal of bromate ion from water using granular activated carbon, Water Res. 33 (1999) 2959–2970.
[4] R. Chitrakar, A. Sonoda, Y. Makita, T. Hirotsu, Calcined Mg-Al layered double hydroxides for uptake of trace levels of bromate from aqueous solution, Ind. Eng. Chem. Res. 50 (2011) 9280–9285.
[5] N. Chubar, New inorganic (an)ion exchangers based on Mg-Al hydrous oxides: (Alkoxide-free) sol-gel synthesis and characterisation, J. Colloid Interface Sci. 357 (2011) 198–209.
[6] K.H. Goh, T.T. Lim, Influences of co-existing species on the sorption of toxic oxyanions from aqueous solution by nanocrystalline Mg/Al layered double hydroxide, J. Hazard. Mater. 180 (2010) 401–408.
[7] K.H. Goh, T.T. Lim, A. Banas, Z.L. Dong, Sorption characteristics and mechanisms of oxyanions and oxyhalides having different molecular properties on Mg/Al layered double hydroxide nanoparticles, J. Hazard. Mater. 179 (2010) 818–827.
[8] C.G. van Ginkel, A.M. van Haperen, B. van der Togt, Reduction of bromate to bromide coupled to acetate oxidation by anaerobic mixed microbial cultures, Water Res. 39 (2005) 59–64.
[9] L. Xie, C. Shang, The effects of operational parameters and common anions on the reactivity of zero-valent iron in bromate reduction, Chemosphere 66 (2007) 1652–1659.
[10] H. Chen, Z.Y. Xu, H.Q. Wan, J.Z. Zheng, D.Q. Yin, S.R. Zheng, Aqueous bromate reduction by catalytic hydrogenation over Pd/Al2O3 catalysts, Appl. Catal. B—Environ. 96 (2010) 307–313.
[11] X. Zhao, H.J. Liu, Y.L. Shen, J.H. Qu, Photocatalytic reduction of bromate at C-60 modified Bi2MoO6 under visible light irradiation, Appl. Catal. B—Environ. 106 (2011) 63–68.
[12] K.H. Goh, T.T. Lim, Z.L. Dong, Application of layered double hydroxides for removal of oxyanions: a review, Water Res. 42 (2008) 1343–1368.
[13] D.G. Evans, R.C.T. Slade, Structural aspects of layered double hydroxides, in: X. Duan, D.G. Evans (Eds.), Layered Double Hydroxides, 2006, pp. 1–87.
[14] R. Chitrakar, Y. Makita, A. Sonoda, T. Hirotsu, Fe-Al layered double hydroxides in bromate reduction: synthesis and reactivity, J. Colloid Interface Sci. 354 (2011) 798–803.
[15] R. Chitrakar, A. Sonoda, Y. Makita, T. Hirotsu, Synthesis and bromate reduction of sulfate intercalated Fe(II)-Al(III) layered double hydroxides, Sep. Purif. Technol. 80 (2011) 652–657.
[16] L. Lv, T. Jiang, S.H. Zhang, X. Yu, Exposure to mutagenic disinfection byproducts leads to increase of antibiotic resistance in pseudomonas aeruginosa, Environ. Sci. Technol. 48 (2014) 8188–8195.
[17] Y. Zhang, X.L. Li, H.Y. Liu, A novel process for bromate removal from water using calcined Zn-Al layered double hydroxides, Desalin. Water. Treat. 55 (2015) 1325–1332.
[18] Y. Zhang, X.L. Li, Preparation of Zn-Al CLDH to remove bromate from drinking water, J. Environ. Eng.—ASCE 140 (2014) 04014018.
[19] Y. Kuroda, Y. Miyamoto, M. Hibino, K. Yamaguchi, N. Mizuno, Tripodal ligand-Stabilized layered double hydroxide nanoparticles with highly exchangeable CO32−, Chem. Mater. 25 (2013) 2291–2296.
[20] K.H. Goh, T.T. Lim, Z.L. Dong, Enhanced arsenic removal by hydrothermally treated nanocrystalline Mg/Al layered double hydroxide with nitrate intercalation, Environ. Sci. Technol. 43 (2009) 2537–2543.
[21] P.D. Yang, D.Y. Zhao, D.I. Margolese, B.F. Chmelka, G.D. Stucky, Generalized syntheses of large-pore mesoporous metal oxides with semicrystalline frameworks, Nature 396 (1998) 152–155.
[22] F.H. Li, H. Fu, J.P. Zhai, Q. Li, Synthesis of mesostructured ferric oxyhydroxides templated by alkyl surfactants: effect of pH, F- and solvents, and their adsorption isotherms for As(V), Microporous Mesoporous Mater. 123 (2009) 177–184.
[23] F.H. Li, X.R. Fu, J. Huang, J.P. Zhai, Synthesis of mesostructured iron oxides with potential As(V) adsorption application, Chem. Res. Chin. Univ. 28 (2012) 559–562.
[24] F.H. Li, D.Y. Nie, Iron-based inorganic mesoporous materials, Prog. Chem. 26 (2014) 961–975.
[25] T. Itoh, N. Ohta, T. Shichi, T. Yui, K. Takagi, The self-assembling properties of stearate ions in hydrotalcite clay composites, Langmuir 19 (2003) 9120–9126.
[26] J. Wang, J.D. Zhou, Z.S. Li, Y. He, S.S. Lin, Q. Liu, M.L. Zhang, Z.H. Jiang, Mesoporous mixed metal oxides derived from P123-templated Mg-Al layered double hydroxides, J. Solid State Chem. 183 (2010) 2511–2515.
[27] B.J. Pan, L.L. Xiao, G.Z. Nie, B.C. Pan, J. Wu, L. Lv, W.M. Zhang, S.R. Zheng, Adsorptive selenite removal from water using a nano-hydrated ferric oxides (HFOs)/polymer hybrid adsorbent, J. Environ. Monit. 12 (2010) 305–310.

[28] S. Mandal, S. Tripathy, T. Padhi, M.K. Sahu, R.K. Patel, Removal efficiency of fluoride by novel Mg-Cr-Cl layered double hydroxide by batch process from water, J. Environ. Sci.—China 25 (2013) 993–1000.
[29] F.H. Li, Layer-by-layer loading iron onto mesoporous silica surfaces: synthesis, characterization and application for As(V) removal, Microporous Mesoporous Mater. 171 (2013) 139–146.
[30] J.S. Valente, M. Sanchez-Cantu, E. Lima, F. Figueras, Method for large-scale production of multimetallic layered double hydroxides: formation mechanism discernment, Chem. Mater. 21 (2009) 5809–5818.
[31] Y.L. Wang, P.X. Wu, Y.W. Li, N.W. Zhu, Z. Dang, Structural and spectroscopic study of tripeptide/layered double hydroxide hybrids, J. Colloid Interface Sci. 394 (2013) 564–572.
[32] V. Rives, Layered Double Hydroxides: Present and Future, Nova Science Publishers, Huntington, N.Y, 2001.
[33] F.R. Costa, A. Leuteritz, U. Wagenknecht, D. Jehnichen, L. Haussler, G. Heinrich, Intercalation of Mg-Al layered double hydroxide by anionic surfactants: preparation and characterization, Appl. Clay Sci. 38 (2008) 153–164.
[34] V. Rives, M.A. Ulibarri, Layered double hydroxides (LDH) intercalated with metal coordination compounds and oxometalates, Coord. Chem. Rev. 181 (1999) 61–120.
[35] K. Nejati, Z. Rezvani, Synthesis and characterisation of nanohybrids of olsalazine-intercalated Al-Mg layered double hydroxide, J. Exp. Nanosci. 7 (2012) 412–425.
[36] D.S. Tong, C.H. Zhou, M.Y. Li, W.H. Yu, J. Beltramini, C.X. Lin, Z.P. Xu, Structure and catalytic properties of Sn-containing layered double hydroxides synthesized in the presence of dodecylsulfate and dodecylamine, Appl. Clay Sci. 48 (2010) 569–574.
[37] X.X. Ruan, S. Huang, H. Chen, G.R. Qian, Sorption of aqueous organic contaminants onto dodecyl sulfate intercalated magnesium iron layered double hydroxide, Appl. Clay Sci. 72 (2013) 96–103.
[38] T. Bujdoso, A. Patzko, Z. Galbacs, I. Dekany, Structural characterization of arsenate ion exchanged MgAl-layered double hydroxide, Appl. Clay Sci. 44 (2009) 75–82.
[39] M. Thommes, B. Smarsly, M. Groenewolt, P.I. Ravikovitch, A.V. Neimark, Adsorption hysteresis of nitrogen and argon in pore networks and characterization of novel micro- and mesoporous silicas, Langmuir 22 (2006) 756–764.
[40] M. Thommes, K. Kaneko, A.V. Neimark, J.P. Olivier, F. Rodriguez-Reinoso, J. Rouquerol, K.S.W. Sing, Physisorption of gases, with special reference to the evaluation of surface area and pore size distribution (IUPAC Technical Report), Pure Appl. Chem. 87 (2015) 1051–1069.
[41] Y.M. Ren, P.X. Liu, J. Feng, J. Ma, Q. Wen, M.L. Zhang, Selective recognition of molybdenum(VI) from water by Mo(VI) oxy ion-imprinted particle as an adsorbent, Chem. Eng. J. 219 (2013) 286–294.
[42] C. Forano, Environmental remediation involving layered double hydroxides, Interface Sci. Technol. 1 (2004) 425–458.
[43] S. Goldberg, Application of surface complexation models to anion adsorption by natural materials, Environ. Toxicol. Chem. 33 (2014) 2172–2180.
[44] A. Bhatnagar, Y. Choi, Y. Yoon, Y. Shin, B.H. Jeon, J.W. Kang, Bromate removal from water by granular ferric hydroxide (GFH), J. Hazard. Mater. 170 (2009) 134–140.
[45] M.A. Ulibarri, I. Pavlovic, M.C. Hermosin, J. Cornejo, Hydrotalcite-like compounds as potential sorbents of phenols from water, Appl. Clay Sci. 10 (1995) 131–145.
[46] Y. Zhang, S. Jing, H.Y. Li, Reactivity and mechanism of bromate reduction from aqueous solution using Zn-Fe(II)-Al layered double hydroxides, Chem. Eng. J. 266 (2015) 21–27.
[47] M.C. Hermosin, I. Pavlovic, M.A. Ulibarri, J. Cornejo, Hydrotalcite as sorbent for trinitrophenol: sorption capacity and mechanism, Water Res. 30 (1996) 171–177.
[48] M.A. Ulibarri, I. Pavlovic, C. Barriga, M.C. Hermosin, J. Cornejo, Adsorption of anionic species on hydrotalcite-like compounds: effect of interlayer anion and crystallinity, Appl. Clay Sci. 18 (2001) 17–27.
[49] G. Mendoza-Damian, F. Tzompantzi, A. Mantilla, R. Perez-Hernandez, A. Hernandez-Gordillo, Improved photocatalytic activity of SnO2-ZnAl LDH prepared by one step Sn4+ incorporation, Appl. Clay Sci. 121 (2016) 127–136.
[50] J.F. Mcintyre, R.T. Foley, B.F. Brown, Ultraviolet-Spectra of aluminum salt-solutions, Inorg. Chem. 21 (1982) 1167–1172.